Published in final edited form as:
Dev Biol. 2006 March 1; 291(1): 38–52. doi:10.1016/j.ydbio.2005.12.003.

The mouse *Ovol2* gene is required for cranial neural tube development

Douglas R. Mackay[a], **Ming Hu**[a], **Baoan Li**[a], **Catherine Rhéaume**[a], and **Xing Dai**[a,b,*]

[a]Department of Biological Chemistry, College of Medicine, D250 Med Sci I, University of California, Irvine, CA 92697-1700, USA

[b]Developmental Biology Center, University of California, Irvine, CA 92697, USA

Abstract

The *Ovo* gene family encodes a group of evolutionarily conserved transcription factors and includes members that reside downstream of key developmental signaling pathways such as Wg/Wnt and BMP/TGF-β. In the current study, we explore the function of *Ovol2*, one of three *Ovo* paralogues in mice. We report that *Ovol2* is expressed during early–mid embryogenesis, particularly in the inner cell mass at E3.5, in epiblast at E6.5, and at later stages in ectodermally derived tissues such as the rostral surface (epidermal) ectoderm. Embryos in which *Ovol2* is ablated exhibit lethality by E10.5, prior to which they display severe defects including an open cranial neural tube. The neural defects are associated with improper *Shh* expression in the underlying rostral axial mesoderm and localized changes of neural marker expression along the dorsoventral axis, as well as with expanded cranial neural tissue and reduced cranial surface ectoderm culminating in a lateral shift of the neuroectoderm/surface ectoderm border. We propose that these defects reflect the involvement of *Ovol2* in independent processes such as regionalized gene expression and neural/non-neural ectodermal patterning. Additionally, we present evidence that *Ovol2* is required for efficient migration and survival of neural crest cells that arise at the neuroectoderm/surface ectoderm border, but not for their initial formation. Collectively, our studies indicate that *Ovol2* is a key regulator of neural development and reveal a previously unexplored role for *Ovo* genes in mammalian embryogenesis.

Keywords

Ovo; *Ovol2*; Neural tube; Brain; *Shh* signaling; Neuroectoderm; Surface ectoderm (epidermal ectoderm); Neural crest

Introduction

The embryonic brain develops from a region of specialized dorsal ectoderm known as the neural plate, within which the specification of the anterior neuroectoderm is initiated by the anterior visceral endoderm and is subsequently maintained by signals from the underlying anterior axial mesendoderm derived from the node (Brennan et al., 2001; Wilson and Houart, 2004). Ectoderm also gives rise to the surface ectoderm, precursor of the epidermis and its appendages. Studies in *Xenopus*, zebrafish, and chick suggest that the induction of neural plate and patterning of neural and non-neural ectoderm are governed by a complex interplay between BMP, Wnt, and FGF signaling pathways (Altmann and Brivanlou, 2001; Bally-Cuif and

*Corresponding author. Department of Biological Chemistry, College of Medicine, D250 Med Sci I, University of California, Irvine, CA 92697-1700, USA. Fax: +1 949 824 2688. xdai@uci.edu (X. Dai).

Hammerschmidt, 2003). Specifically, a BMP signaling gradient, set forth by BMPs and their antagonists, is proposed to differentially pattern the ectoderm; inhibition of BMP activity induces a neural fate, high BMP activity specifies an epidermal fate, and intermediate BMP activity induces the formation of neural crest cells at the neural/non-neural border (Hemmati-Brivanlou and Melton, 1997; Marchant et al., 1998; Nguyen et al., 1998; Wilson et al., 1997). Additionally, FGF signaling promotes a neural fate, whereas active Wnt signaling inhibits the ectoderm's response to FGF signaling, thereby permitting epidermal specification (Wilson et al., 2001;Wittler and Kessel, 2004). Also implicated in this process, largely by studies in *Xenopus*, are transcription factors that either promote (e.g., the Zic family members) or inhibit (e.g., Msx1, Dlx3) neural plate differentiation (Feledy et al., 1999; Kuo et al., 1998; Luo et al., 2001; Mizuseki et al., 1998; Nakata et al., 1997; Suzuki et al., 1997). To date, little is known about the genetic pathways underlying neural/epidermal patterning in mammals, as studies have been hampered by the in utero development of embryos and by functional redundancy between multiple members of particular gene families.

A number of important signaling centers are formed to elaborate anterior–posterior (A–P) and dorsal–ventral (D–V) patterning of the prospective brain (reviewed in Joyner, 2002; Rubenstein and Beachy, 1998). The rostral domain of axial mesendoderm including the prechordal plate specifies the ventral aspect of the cranial neuroectoderm, while the surface ectoderm adjacent to the neural plate emanates BMP signals that specify a dorsal neural fate. The balance between these opposing activities determines the final D–V specification of the cranial neural tube (Joyner, 2002). Shh is an important ventralizing signal from the prechordal plate and the notochord. It induces the expression of itself and of *Ptch1*, encoding an Shh receptor and inhibitor, in the ventral neuroectoderm, as well as the expression of ventral forebrain markers such as the transcription factor Nkx2.1 (Briscoe and Ericson, 2001; Dale et al., 1997; Goodrich et al., 1997; Jessell, 2000; Shimamura and Ruben-stein, 1997). In the dorsal neuroectoderm, transcription factors Pax3 and Msx1/2 are expressed in response to dorsalizing BMP signals and are required for dorsal neural differentiation (Goulding et al., 1993; Liem et al., 1995). Understanding the function of known and yet uncharacterized transcription factors and how they interact with the morphogenetic signaling events is key to understanding the genetic networks that underlie the formation of complex tissues such as the brain.

Cranial neurulation is an integral component of brain morphogenesis. This process requires morphogen-induced cell shape changes and movements, a delicate balance between proliferation and apoptosis in the neuroepithelium, expansion of the cranial mesoderm, and efficient migration of neural crest cells away from the neural plate (Copp et al., 2003). Disruption of any of these cellular and morphological events leads to exencephaly, ultimately resulting in defective brain formation. The medial expansion of the surface ectoderm provides a major driving force for folding and subsequent closure of the neural plate (Smith and Schoenwolf, 1997). Genetic studies in mice have elucidated a critical involvement of a number of genes in cranial neurulation (Copp et al., 2003; Smith and Schoenwolf, 1997), including *twist*, which encodes a basic helix–loop–helix protein expressed in head mesenchyme, and the transcription factor AP-2, which is expressed in cranial surface ectoderm. Thus, factors present outside of the neuroepithelium can also affect the morphogenesis of the cranial neural tube.

The *Ovo* gene family encodes evolutionarily conserved zinc-finger transcription factors whose function in embryogenesis is under-explored. The founding member of this family, *Drosophila ovo*, is required for epidermal denticle formation and oogenesis and has been shown to be genetically downstream of canonical Wg/Wnt signaling (Mevel-Ninio et al., 1995; Oliver et al., 1994; Payre et al., 1999). *lin-48*, the *ovo* homologue found in *C. elegans*, is required for cell fate specification during hindgut development (Chamberlin et al., 1999). There are three *ovo* homologues in mammals, designated *Ovol1*, *Ovol2*, and *Ovol3*. In mice, *Ovol1* is required for hair follicle differentiation, where it is regulated by nuclear effectors of Wnt signaling, and

also for kidney and male germ cell development (Dai et al., 1998; Li et al., 2002b, 2005). Recently, human *OVOL1* has been identified as a gene that is responsive to TGF-β1/BMP7 treatment via a Smad4-dependent pathway (Kowanetz et al., 2004). That members of the *ovo* gene family act downstream of signaling pathways required for diverse processes during both early and late stages of embryonic development raises the possibility that *ovo* genes might be important for embryogenesis.

Previous studies revealed *Ovol2* expression in brain, testis, and epithelial tissues such as skin and intestine of adult mice (Li et al., 2002a). In this study, we show that it is also expressed during early–mid embryogenesis, particularly in the epiblast and its ectodermal derivatives in the developing head. Using a gene targeting approach, we ablated *Ovol2* expression and observed that *Ovol2* is required for the development of the embryonic brain. We further demonstrate that *Ovol2* is required for maintaining the proper expression of signaling molecules such as *Shh* and *Wnt1* along the cranial D–V axis, for positioning the neuroectoderm/surface ectoderm border in the head region, for maintenance of migrating neural crest cells, and for closure of the cranial neural tube.

Materials and methods

Generation of Ovol2 mutant mice

A 120 kb BAC clone containing the *Ovol2* locus was identified by screening a 129/Sv genomic library (Incyte Genomics) and was used to generate a targeting vector designed to delete exons 1a, 1b, and 2 (E1A, E1B, E2) that contain the start codon of the Ovol2 open reading frame (Fig. 1A; Li et al., 2002a). A 2 kb *Bam*HI fragment corresponding to the genomic region upstream of E1A was cloned as the 5′ arm into the pPGKneobpA-lox2PGKDTA vector at the *Hin*dII site by blunt-end ligation. Primers corresponding to sequences in E2 and E3 were used to amplify a 14 kb genomic sequence which was subsequently cloned into the TOPO-TA vector (Invitrogen). A 6.8 kb *Pst*I fragment was released from the resulting plasmid and blunt-end ligated into the *Not*I site of the targeting vector as the 3′ arm. A 1 kb *Sma*I–*Afl*II fragment encoding the EGFP protein (from pEGFP-N1, Clontech) was inserted downstream of the 5′ arm at the *Nhe*I site by blunt-end ligation.

The targeting vector was linearized with *Sac*II and electroporated into E14 embryonic stem (ES) cells. After selection in the presence of G418, clones were screened by PCR and Southern hybridization (Figs. 1B–D), two of which were injected into blastocysts. The resulting chimeras were mated with wild-type C57BL/6J females to produce F1 progeny of a C57BL6/J×129Ola (B6×129) mixed genetic background, which were further intercrossed to produce homozygous mutant F2 progeny for study. Subsequent breeding of F1 heterozygous males with wild-type CD1 outbred females generated heterozygous offspring enriched in a CD1 background that were also used to produce homozygous mutant mice for study. Mutant phenotypes in mice derived from both ES clones were identical.

PCR genotyping, Southern blot, and RT-PCR analysis

Genomic DNA or lysate isolated from ES cells, tail clippings, or yolk sacs was used for PCR genotyping using the following primer sequences (designated as arrows in Fig. 1A): PCRi: 5′-TGCTTCGTGGGTTGGCCTGAGAAC-3′ and 5′-CAGATGTCCATCGGTGCCTTGGGC-3′; PCRii: 5′-GTTTCGCTTGGTGGTCGAATGGGCAG-3′ and 5′-CACCACAGAGGCTGGGAGTGACATC-3′; PCRiii: 5′-CGCTCCTTCTTTCTAGCAAGTCTCCCG-3′ and 5′-AAGTCGTGCTGCTTCATGTG-3′; PCRiv: 5′-GCTGACCCTGAAGTTCATCTGACCA-3′ and 5′-CGCTTCTCGTTGGGGTCTTTGCTCA-3′. Southern blot analysis was performed essentially

as described (Sambrook and Russell, 2001) using the probe indicated in Fig. 1A. RT-PCR was performed using RNA isolated from either single embryos (Superscript One-Step RT-PCR with Platinum *Taq* kit, Invitrogen) or pooled embryos (Superscript III Reverse Transcriptase, Invitrogen) according to the manufacturer's recommendations. The following primer sequences were used to detect *Ovol2* transcripts: 5′-CCCACCATGCCCAAAGTCTTTCTGGTA-3′ and 5′-GGCGTCGTGAAGCTCTGGAGTTTCAG-3′ or 5′-GAGCCTGGGCTGTCTGCTCCGCG-3′ and 5′-CCCAAGCTTCGCTGCCAGATGTCCATCGGTGC-3′. Primers specific for *Gapdh* were used as a control.

Embryological techniques and histology

For morphological analysis, embryos were dissected at the appropriate stages, removed from the yolk sac, fixed for 1–2 h at 4°C in 4% paraformaldehyde/PBS, and washed in PBS. Pictures were taken using a Spot-RT camera mounted on a Leica MZFLIII dissecting microscope equipped with a GFP filter. GFP images were similarly acquired, except that the embryos were unfixed at the time of analysis. For histological analysis, whole deciduae at the appropriate stages were removed from the uterus, fixed for 2 h at room temperature in Bouin's fixative, and subsequently washed in 70% ethanol until embryos were clear. Following dehydration and embedding in paraffin, 5 μm sections were cut and stained with hematoxylin and eosin.

Whole mount in situ hybridization

Embryos were dissected at the indicated stages, fixed for 2 h at 4°C in 4% paraformaldehyde/PBS, dehydrated through a series of increasing methanol concentrations, and stored at −20°C. Mutant embryos in both B6×129 and CD1-enriched backgrounds that showed severe neural fold rounding at E8.5 were used for final analysis along with stage-matched controls. Whole mount in situ hybridization was performed essentially as described (Nagy et al., 2003). For select probes, OCT sections (14 μm) were prepared after hybridization for further analysis. The following probes were transcribed using either T7, T3, or Sp6 RNA polymerase (T7 and Sp6, New England Biolabs; T3, Stratagene): *Ovol2* (GenBankAY0990537); *Shh* (Echelard et al., 1993); *Otx2* (Ang et al., 1996); *Fgf8* (Mahmood et al., 1995); *Krox20* (Wilkinson et al., 1989); *Ptch1* (Goodrich et al., 1996); *Wnt1* (Parr et al., 1993); *Nkx2.1* (Camus et al., 2000); *Pax3* (Goulding et al., 1991); *Msx1* (Catron et al., 1996); *Msx2* (Catron et al., 1996); *Wnt6* (Parr et al., 1993); *Dlx3* (Morasso et al., 1996); and *Sox10* (Pusch et al., 1998).

BrdU incorporation and immunological staining

Proliferating cells in the embryo were labeled by injecting pregnant female mice with 50 μg BrdU/g body weight 30 min before dissection. Embryos were dissected in PBS and fixed for 1–2 h in 4% paraformaldehyde/PBS, equilibrated in 30% sucrose, and frozen in OCT. Frozen sections (12–14 μm) were stained with an anti-BrdU monoclonal antibody (Roche) as previously described (Li et al., 2005). Antibodies against Ki67 (Vector Laboratories) and phosphorylated histone-H3 (Upstate Biotechnology) were used to stain frozen sections using standard immunostaining protocols. The number of phospho-H3-positive nuclei in the neuroectoderm was counted from serial sections and compared to the total number of cells as determined by DAPI-positive nuclei.

Nile blue sulfate staining and TUNEL assay

Nile blue sulfate staining was performed essentially as described (Anderson et al., 2002), except that embryos were stained for 1 h on ice. The TUNEL assay was performed on whole embryos fixed in 4% paraformaldehyde using the In Situ Cell Death Detection Kit (Roche), according to the manufacturer's recommendations.

Results

Ovol2 is required for embryonic development

To understand the biological role of *Ovol2*, we used homologous recombination in embryonic stem (ES) cells to ablate the murine *Ovol2* gene. We replaced the initial three exons of *Ovol2* with a cassette containing the EGFP and neo^r genes, which would result in EGFP expression being controlled by the *Ovol2* promoter region (Fig. 1A). The targeting construct was electroporated into ES cells followed by selection with G418, yielding two independently targeted clones that were injected into blastocysts and gave germline transmission (Figs. 1B–D). No homozygous *Ovol2* mutant pups were recovered from heterozygote intercrosses in either the B6×129 or the CD1-enriched genetic backgrounds examined (Table 1). Further analysis of embryonic litters at various stages indicated that *Ovol2* mutant embryos died around embryonic day 10.5 (E10.5; Table 1), and χ^2 analysis of genotype distributions at earlier stages of development revealed no significant deviation from the expected Mendelian ratios (data not shown). Thus, these data indicate that *Ovol2* is required for embryonic development before E10.5.

Widespread expression of Ovol2 during early–mid embryogenesis

To identify the tissues whose development might be affected by loss of *Ovol2*, we analyzed its spatio-temporal expression during early–mid embryonic development. RT-PCR analysis revealed that *Ovol2* is expressed in ES cells and E7.5, E8.5, E9.5, and E10.5 wild-type embryos (Fig. 2A). EGFP fluorescence in heterozygous *Ovol2* embryos was examined as a read-out of *Ovol2* promoter activity. EGFP expression was detected in the inner cell mass of blastocysts (Fig. 2B) and later in the epiblast but not the extraembryonic region of E6.5 embryos (Fig. 2C). As development progressed, EGFP protein continued to be present broadly in epiblast-derived tissues, with enhanced fluorescence in what appear to be anterior definitive endoderm and axial mesoderm (arrowhead and arrow in Fig. 2F, respectively) and no expression in the visceral endoderm (Figs. 2D–F). By ~E8.5, EGFP fluorescence became more restricted and was observed in the cephalic neural folds (arrow), the surface ectoderm bordering the neural plate (arrowheads), and the gut tube (open arrowhead), but not in the developing heart (*; Figs. 2G–H).

Whole mount in situ hybridization was then performed using *Ovol2* antisense probes. *Ovol2* transcripts were detected in E8.75 embryos in the gut tube endoderm and in the surface ectodermal component of the head and the newly formed first branchial arch, but not in heart (Figs. 2I–K). At E9.5, *Ovol2* expression was observed in the forebrain area, as well as in the branchial arches, otic vesicles, developing gut, and at low levels throughout the entire embryo (Figs. 2L, N–P). No hybridization signal was observed in stage-matched *Ovol2* mutant embryos at E8.75 or at E9.5 (Fig. 2M and data not shown), indicating that the signals observed in the wild-type embryos are specific to *Ovol2* and that the mutant allele generated in the present study likely represents a null allele. Moreover, the similarity in the distribution of *Ovol2* transcripts and EGFP fluorescence confirms that the presence of EGFP protein is a good indicator of the endogenous pattern of *Ovol2* expression.

Ovol2 is required for cranial neural, gut, and heart development

We next performed a detailed morphological analysis of *Ovol2* mutant embryos at different stages prior to death. Initial analyses were performed on F2 homozygous mutants from F1 heterozygote intercrosses in a mixed B6×129 genetic background. Given the expression of *Ovol2* in the presumptive forebrain area and in the surface ectoderm adjacent to the cranial neuroectoderm, we first focused on the developing brain. The earliest, most consistent signs of morphological defects were detected in mutant embryos at ~E8.5–8.75, when they displayed larger, more rounded neural folds (white arrowheads; Figs. 3A–B, D–E). Optic invaginations,

which normally occur at this stage, were not observed in the mutant (black arrowheads in Figs. 3A, D). These defects were not due to a general delay in development as the mutant and wild-type embryos analyzed possessed the same number of somites. The rounded neural folds in the E8.5 mutant embryos were more evident at a histological level. In wild-type embryos, a sharp transition from neuroectoderm to surface ectoderm was observed, and there was a clear morphological distinction between these two adjacent epithelia (Fig. 3G). In the mutant, however, the neuroectoderm was expanded and folded laterally towards the surface ectoderm, as identified by its thin appearance, resulting in an apparent lateral shift of the neuroectoderm/surface ectoderm junction (Fig. 3H). The transition from the columnar epithelial morphology of the neuroectoderm to the cuboidal epithelium of the surface ectoderm was not as distinct in the mutant and appeared to be more gradual (see insets in Figs. 3G–H). By E9.5, all of the mutant embryos displayed a failure of cranial neural tube closure, as well as a failure of the turning process (Fig. 3F; compare to 3C). There was no evidence of formation of the optic eminence or otic pit in the mutant, and the branchial arches were often underdeveloped. By E10.5, most mutant embryos were fully resorbed, leaving empty yolk sacs that appeared deflated and seemed to lack proper vascularization (data not shown).

A similar cranial phenotype was observed when the mutant allele was bred into a CD1-enriched genetic background (Figs. 3I–N). Sectioning through these mutant embryos revealed that, at E9.5, their forebrain developed as two separate hollow tubes instead of forming a single vesicle (Fig. 3O). There was a severe paucity of cranial mesenchyme (*) and no sign of surface ectoderm covering the forebrain region. We should note that the apparent expressivity of the neural phenotype was lower in this background than that observed in the B6×129 background. For example, not all mutant embryos in the CD1-enriched background showed a dramatic rounding of their neural folds at E8.5, and rudimentary optic and otic structures were often seen at E9.5 (data not shown). Furthermore, most mutant embryos were able to turn by E9.5, although they displayed a twisted body axis with multiple kinks (Figs. 3F, N; also see Fig. 5G). Surprisingly, we recovered a single mutant at E9.5 showing a rather normal external appearance, with near-normal head morphology, body shape, and sensory structures. However, this “escaper” still displayed areas of open cranial neural tube as well as open regions in trunk neural tube (spina bifida; Fig. 3P).

Consistent with *Ovol2* expression in the developing gut tube, histological analysis revealed abnormal gut morphology in the *Ovol2* mutants, the extent of which was not significantly affected by strain background (Fig. 3H, data not shown). Overall, the mutant gut epithelium appeared less developed than the wild-type, and foregut often lacked the eosin-positive acellular debris normally found within the wild-type lumen. Marker expression studies (Mackay and Dai, unpublished) further suggested that the differentiation of the hindgut endoderm is delayed in the *Ovol2* mutant.

While *Ovol2* expression was not detected in the developing heart tube at E8.5, all mutant embryos at this stage displayed severely defective heart development (Figs. 3D–F). Similar to neural development, the heart phenotype was slightly more severe in the B6×129 background than that in CD1. Compared to wild-type E8.5 embryos that had a single linear or already looped heart tube, the somite-matched mutant embryos either displayed a failure in the fusion of the left and right heart primordia or lacked any sign of heart primordium altogether. This cardia bifida phenotype was confirmed at a histological level, where it was clear that in some mutants the two heart fields failed to fuse properly (arrows in Figs. 4B–C). As development progressed, mutant hearts were able to form a single heart tube but were much smaller than their wild-type counterparts and showed abnormal patterns of looping morphogenesis and septation, resulting in a single ventricular chamber abutted by two laterally positioned atrium-like structures (Figs. 4D–M). Moreover, the mutant hearts displayed an apparently dilated indistinct atriosinus region (*; compare Figs. 4M to I) and an indistinct outflow tract/aortic sac

region (arrows; compare Figs. 4J to F). These severe heart defects in the mutants would be expected to result in an embryonic heart failure, which was most likely the cause of the subsequent embryonic death.

Ovol2 mutant embryos show mild defects in signaling centers involved in D–V brain patterning

Correct A–P and D–V patterning re essential for neural development and neural tube closure (Joyner, 2002). We first examined A–P brain patterning by performing whole mount in situ hybridization using a panel of probes marking particular regions of the developing brain along the A–P axis. *Otx2* is normally expressed in the neuroectoderm and anterior mesendoderm of the developing forebrain and midbrain and is essential for the proper patterning of anterior neural tissues (Ang et al., 1996). Wild-type embryos showed an expected pattern of *Otx2* expression, and *Otx2* expression in *Ovol2* mutant embryos was not significantly different, indicating that the forebrain and midbrain domains were specified properly in the absence of *Ovol2* (Fig. 5A). Further experiments using probes for *Fgf8*, expressed in the anterior neural ridge located at the rostral margin of the neural plate and the isthmic organizer located at the midbrain/hindbrain boundary (Mahmood et al., 1995), and *Krox20*, expressed in the hindbrain (Wilkinson et al., 1989), confirmed that A–P brain patterning was not significantly affected in *Ovol2* mutants (Figs. 5B–C).

To examine D–V patterning of the developing mutant brain, we performed in situ hybridization using a probe for *Shh*. At E8.5, *Shh* is normally expressed in the axial mesoderm of the notochord and prechordal plate (arrow in Fig 5D, top panel) and later in the ventral aspect of the brain (arrowhead in Fig. 5E, top panel). In *Ovol2* mutant embryos, *Shh* expression in the notochord appeared normal; however, the prechordal plate region marked by *Shh* was not as rostrally extended as seen in the wild type and lacked the characteristic hook-shaped morphology (arrows in Figs. 5D–E). In addition, *Shh* expression appeared more diffuse in the truncated prechordal plate region and was weaker in the ventral forebrain of the mutants (Figs. 5E–F). As the embryos developed further, the defects in prechordal plate and ventral forebrain became more pronounced as the domain of *Shh* expression was not properly maintained (Fig. 5G; arrowhead indicates a gap within the *Shh* expressing domain of mutant ventral forebrain). Additionally, the notochord in the mutants displayed multiple kinks (* in Fig. 5G), which further indicated that the body axis was twisted or improperly extended. Expression of *Ptch1* appeared diffuse in the mutant ventral brain (Fig. 5H), likely due to the improper distance from the source of *Shh* signal. We next examined the expression of *Wnt1*, which is normally localized to the dorsal aspect of the cranial neural folds of the midbrain region (Parr et al., 1993). As expected, wild-type embryos expressed *Wnt1* in a spatially restricted area adjacent to the neuroectoderm/surface ectoderm junction (Figs. 5I–J). In the mutants, however, the domain of *Wnt1* expression was expanded ventrally, although a dorsal concentration was still evident (Figs. 5I–J). Additionally, the dorsal boundary of *Wnt1* expression was shifted laterally, consistent with the apparent shift of the neuroectoderm/surface ectoderm border observed at a morphological level (see arrowheads in Figs. 3H and 5J). Taken together, these results indicate that the loss of *Ovol2* does not affect A–P patterning of the brain but leads to slightly altered expression of signaling molecules that are known to be involved in D–V patterning of the neural tube.

Expansion of neuroectoderm and reduction of surface ectoderm culminates in a lateral shift of the mutant cranial neuroectoderm/surface ectoderm border

To examine whether D–V specification is disrupted in the *Ovol2* mutant brain, we investigated the expression of several well-characterized D–V neural markers. The expected ventrally or dorsally localized expression of *Nkx2.1*, *Pax3*, *Msx1*, and *Msx2* in the cranial neural tube suggests that the overall D–V domains were largely maintained in the *Ovol2* mutant (Figs. 6A–

B and data not shown). Remarkably, *Msx2* and *Pax3* expression showed a similar lateral shift towards the presumptive surface ectoderm (Figs. 6A–B), as observed for *Wnt1* expression.

The lateral shift of dorsal neural markers in the mutant, together with the apparent increase in the contour of the neuroectoderm, suggests that mutant neuroectoderm is expanded. At least three possibilities may account for such an expansion: overspecification of a neuroectodermal fate at the cost of a surface ectodermal fate, increased neuroectodermal proliferation, and/or decreased neuroectodermal apoptosis. To address whether the surface ectoderm is specified properly in the mutant, we investigated the expression of a surface ectoderm marker, *Wnt6*. *Wnt6* expression was observed in the mutant in the presumptive surface ectoderm that juxtaposes the dorsal border of the neural plate, indicating that *Ovol2*-deficient ectoderm was able to differentiate into surface ectoderm (Fig. 6C). However, the ratio of the cranial surface ectoderm to neuroectoderm was reduced two-fold in the mutants compared to that observed in the wild type (Fig. 6D; $P < 0.0001$). Therefore, a concomitant expansion of neuroectoderm and reduction of surface ectoderm in the mutant contributes to the observed lateral shift of the cranial neuroectoderm/surface ectoderm border.

This phenotype is reminiscent of that observed in *Xenopus* and zebrafish when *Dlx3* function was disrupted (Woda et al., 2003). To address whether *Dlx3* expression is affected in *Ovol2* mutant, we performed whole mount in situ hybridizations using a *Dlx3* probe on E8.5 embryos. Previous studies reported *Dlx3* expression in the first and second branchial arches in mouse embryos at E9.5 (Robinson and Mahon, 1994) and weakly in the rostral ectoderm at E8.0 (Quint et al., 2000). Consistent with these reports, we observed strong *Dlx3* expression in the first branchial arch and weak expression in the cranial surface ectoderm in wild-type E8.5 embryos. Compared to their wild-type littermates, all seven mutant embryos examined displayed much weaker expression in comparable regions, with the difference most apparent when color development for whole mount in situ hybridization was prolonged to enhance the surface ectoderm signal (Figs. 6E–G). These results indicate that a functional *Ovol2* is required for *Dlx3* expression in these areas.

To assess a possible contribution of proliferation to neuroectoderm expansion, we next analyzed the extent of proliferation in the neuroectoderm at E8.5. Widespread proliferation was detected using BrdU labeling and immunological staining for Ki67 in both wild-type and mutant embryos, consistent with rapid growth at this stage of development (data not shown). We instead determined the mitotic index using an antibody that recognizes phosphorylated histone H3, a marker for cells in mitosis (Gurley et al., 1978). The mitotic index was calculated as the ratio of the number of cells in the neuroectoderm that stained positive for phosphorylated histone H3 over the total number of cells in the neuroectoderm as determined by DAPI staining (Figs. 7A–B). We observed regional variability in both the wild-type and mutant embryos, so we averaged the mitotic index over multiple serial sections. Analysis of either the cranial region alone or both cranial and caudal regions combined revealed no increase in mitotic index (Fig. 7B and data not shown). Instead, we observed a slight but statistically significant ($P = 0.037$) decrease in the rate of proliferation in the mutant neuroectoderm.

We also investigated the status of apoptosis in the neuroectoderm at E8.5. Using both Nile blue sulfate staining (Anderson et al., 2002) and TUNEL assays, we did not detect any significant difference in the number of apoptotic cells in wild-type and mutant neuroectoderm at this stage (Fig. 7C and data not shown). Collectively, our data exclude overproliferation or decreased apoptosis as likely causes of cranial neural expansion in the mutant but instead suggest that the lateral shift of the neuroectoderm/surface ectoderm border is a consequence of the expansion of neuroectoderm at the cost of surface ectoderm in the cranial region.

Ovol2 is required for neural crest maintenance and emigration

The mispositioning of the neuroectoderm/surface ectoderm border in *Ovol2* mutants raises the possibility that border cell fates might be affected. The best characterized cell type arising at the border is neural crest cells that undergo an epithelial–mesenchymal transition, delaminate from the neuroepithelium, and migrate away from the neural plate border to various predetermined target locations (Gammill and Bronner-Fraser, 2003). Upon morphological examination, we noticed that cells with neural crest morphology were present in mutant E8.5 embryos, except that they clustered next to the neuroectoderm/surface ectoderm border (see arrow in Fig. 3H). Furthermore, we observed a similar characteristic pattern of apoptosis along the cranial neuroectoderm/surface ectoderm border of both wild-type and mutant E8.5 embryos, previously implicated as from apoptotic neural crest cells (Graham et al., 1994; Trainor et al., 2002). Therefore, it appears that neural crest formation is initiated in the mutant (see below). However, when Nile blue staining was performed on E9.5 embryos, a dramatic increase in the number of apoptotic cells was observed in the mutant, particularly in forebrain, branchial arch, and trunk regions (Figs. 7D–F, H–J). TUNEL assays, while not as sensitive as the Nile blue staining in our hands, confirmed that apoptosis was indeed elevated in the mutant (Figs. 7G, K). The distribution of these apoptotic cells in *Ovol2* mutant embryos is reminiscent of that of migrating neural crest cells.

To directly assess the neural crest population in *Ovol2* mutants, we next examined the expression of *Sox10*, which marks migrating neural crest cells (Cheng et al., 2000; Pusch et al., 1998). At E8.5–E8.75, largely normal but slightly enhanced *Sox10* expression was observed in the mutant embryos, confirming that neural crest cells are specified and formed (Fig. 8A). A detailed analysis of sections revealed that the *Sox10*-expressing cells were displaced laterally towards the surface ectoderm, consistent with the lateral shift of neuroectoderm/surface ectoderm boundary (Fig. 8D). Furthermore, *Sox10*-positive cells still appeared to be an integral part of the neuroectoderm in the mutant, suggesting that their emigration was not efficient. This notion is consistent with the morphological finding of clustered neural crest cells next to the neuroectoderm/surface ectoderm border (see above). By E9.5, the mutants displayed regions of *Sox10* expression that appeared smaller, and either more (compare i in Figs. 8B–C) or less (compare ii in Figs. 8B–C) intense than the wild type. Additionally, the mutants displayed either missing or ectopic regions of *Sox10*-expressing neural crest cells (arrows in Figs. 8B–C). Sectioning through the embryos indeed revealed the presence of condensed clusters of *Sox10*-expressing cells in the mutant, some of which failed to leave the region immediately adjacent to the laterally shifted neuroectoderm/surface ectoderm border (arrowheads in Fig. 8E). Taken together, these results suggest that neural crest maintenance and migration are disrupted in the absence of *Ovol2*.

Discussion

In this study, we uncovered a previously unsuspected function of *Ovol2* in early–mid embryogenesis. Our data demonstrate that a functional *Ovol2* gene is required for the proper development of multiple tissues including brain, neural crest, gut tube, and heart. Presently, our studies do not unequivocally distinguish primary defects from those that arise as secondary consequences of the initial tissue defect, particularly because *Ovol2* expression in early embryos is rather ubiquitous and only gradually becomes restricted to specific tissues or sites. While several independent cellular and molecular mechanisms might underlie the cranial neural tube defect, the major focus of this work (see below), the gut defects might arise as a direct effect of loss of *Ovol2* expression in the developing gut endoderm. Little or no *Ovol2* expression was detected in the developing heart at the time when it was affected, raising the possibility that this defect might be secondary. In this context, we note that over-emphasized anterior neural development, which was observed in these mutants, has been shown to interfere

with heart development (Fishman and Chien, 1997; Jacobson, 1960). Alternatively, the heart defect may be a result of improper neural crest migration and maintenance as it is known that a specific population of neural crest cells, known as the cardiac neural crest, contributes to the development of the outflow tract and possibly other parts of the developing heart (Stoller and Epstein, 2005). Finally, it is possible that *Ovol2* is expressed in heart precursor cells at earlier stages of development and is required for heart tube formation and looping morphogenesis.

Ovol2 and ventral signaling

The ventral midline emanates important signals that pattern the developing neural plate along the A–P and D–V axis. The loss of *Ovol2* led to a defective pattern of *Shh* expression in the rostral domain of the axial mesoderm. Curiously, while EGFP fluorescence suggested *Ovol2* expression in the ventral midline tissues at the headfold stage, *Ovol2* transcripts were not detected in the prechordal plate or notochord after E8.5, yet the extent of disruption of *Shh* expression in these axial structures was more severe at E9.5 than at E8.5. Therefore, it remains to be addressed whether the improper rostral extension of *Shh* expression is a direct effect of loss of *Ovol2* in the axial structures.

Consistent with the prevailing notion that Shh signaling from the prechordal plate induces *Shh* expression in the neuroectoderm of the ventral brain (Shimamura and Rubenstein, 1997), mutant embryos displayed a reduced level of *Shh* expression in the ventral forebrain, likely due to improper Shh signaling from the prechordal plate. However, the expression of several well-known D–V markers appeared grossly normal in *Ovol2* mutant neuroectoderm. Specifically, the expression of ventral markers such as *Ptch1* and *Nkx2.1* was induced in a ventrally restricted fashion. Furthermore, dorsal markers such as *Pax3* and *Msx1/2* were restricted to the dorsal domain of the E8.5 mutant cranial neural tube, confirming that the ventralizing signals were sufficient to repress the expression of these genes in the ventral domain (Liem et al., 1995). Instead, we observed rather specific and local changes in gene expression. For example, we consistently observed ectopic sites of *Ptch1* and *Nkx2.1* expression in the mutant brain, too weak and diffuse to clearly document. Additionally, *Wnt1*, a gene whose expression is normally confined to the dorsal aspect of the neuroectoderm, was abnormally expanded into the ventral domain of the mutant neuroectoderm. Since we observed no significant increase in the expression levels of BMP2 and BMP4 – candidate dorsalizing signals – in the mutant (data not shown), we surmise that the ventral expansion of *Wnt1* expression is likely due to compromised repression from sub-optimum ventral Shh signaling but not over-emphasized dorsalizing signals (Basler et al., 1993; Dickinson et al., 1995; Goulding et al., 1993; Kanzler et al., 2000). This notion is also more in line with the observed reduction (not increase) in the area of surface ectoderm, thought to be the source of dorsalizing signals (Dickinson et al., 1995; Lee and Jessell, 1999; Liem et al., 1995). This said, we cannot rule out the possibility that the expression of other BMPs (e.g., BMP7) or that the downstream components of BMP signaling are somehow affected, leading to a change in BMP activity gradient across the neuroectoderm D–V axis. Collectively, our studies demonstrate that the loss of *Ovol2* leads to local changes in the expression of specific signaling molecules and transcription factors but not a general disruption of D–V patterning in the developing brain. The mid-gestation lethality of *Ovol2* mutants precludes a detailed analysis of specification of ventral neural fates to evaluate the consequence of the observed gene expression defects. Future studies using a conditional *Ovol2* allele to bypass the lethality issue will likely be informative.

Ovol2 and patterning of the neural and non-neural ectoderm

Another interesting and likely independent consequence of *Ovol2* ablation is the lateral shift of the neuroectoderm/surface ectoderm border in the dorsal aspect of the rostral neural tube. This is apparent at a histological level and is confirmed by expression studies of neuroectoderm and surface ectoderm markers. Quantitative analysis of the relative linear dimensions of these

ectodermal derivatives indicates that the neuroectoderm is expanded, while surface ectoderm is reduced in the cranial region of the mutant embryos. These results suggest that *Ovol2* is involved in patterning the neural and non-neural ectoderm, a role that is consistent with its expression in the ectoderm at early stages of embryogenesis. Specifically, *Ovol2* appears to function as an anti-neural gene (see below), where its absence in the ectoderm leads to over-specification of a neural fate. To our knowledge, this work represents the first example elucidating the functional involvement of a transcription factor in patterning the neural and epidermal ectoderm in mice.

The lateral and ventral expansion of *Wnt1* expression in the mutant neuroectoderm deserves more attention. Genetic studies in mice suggested that *Wnt* signaling, via redundant functions of *Wnt1* and *Wnt3a* in the dorsal neural midline, is required for proliferation or survival of dorsal neural precursor cells, including the neural crest, and/or for maintaining a stable dorsal neural fate (Dickinson et al., 1994; Ikeya et al., 1997; Saint-Jeannet et al., 1997). It may be possible that this expanded *Wnt1* expression causes the lateral shift of the neuroectoderm/surface ectoderm border by promoting dorsal neuroectodermal proliferation (Dickinson et al., 1994); however, we consider this possibility highly unlikely due to the following reasons: (1) we observed decreased proliferation in the mutant neuroectoderm, contradictory to the expected effect of *Wnt1* in dorsal ectoderm, and (2) it has been shown that contact with the surface ectoderm can induce ectopic *Wnt1* expression in the neuroectoderm (Liem et al., 1995), suggesting that formation of the neuroectoderm/surface ectoderm border precedes border-specific expression of *Wnt1*. Furthermore, induction of neural crest, a border-specific cell type, can occur without *Wnt1* and *Wnt3a* (Basler et al., 1993; Dickinson et al., 1995; Goulding et al., 1993). Therefore, we favor the hypothesis that the lateral shift of the mutant neuroectoderm/surface ectoderm border reflects a primary defect in neural/non-neural patterning and that the lateral shift of *Wnt1* expression is simply a consequence of an expanded neural plate, which pushes the border and its associated gene expression laterally.

The anti-neural function of *Ovol2* resembles that of *Xenopus*/ zebrafish *Dlx3*, which encodes a homeodomain transcription factor. Loss of *Dlx3* leads to an expansion of neuroectoderm at the expense of surface ectoderm, resulting in mispositioning of the neural/non-neural border (Woda et al., 2003). *Dlx3*, like *Ovol2*, is first expressed broadly throughout embryonic ectoderm and then becomes restricted to the non-neural ectoderm (Woda et al., 2003). The current model states that *Dlx3* functions by repressing the expression of anterior proneural genes, whereby directing or permitting ectoderm to adopt a non-neural fate in response to developmental signals such as Wnt and BMP (Beanan et al., 2000; Feledy et al., 1999). Unlike another anti-neural gene, *Msx1*, which is an immediate-early target of BMP signaling, activation of *Dlx3* expression requires additional factors that are synthesized following BMP signaling (Feledy et al., 1999). It is tempting to speculate that the Ovol2 protein may be one such factor that is required to activate *Dlx3* expression in surface ectoderm and its precursor cells, a notion supported by the significant reduction of *Dlx3* expression in *Ovol2* mutant embryos.

It is important to note that a similar function has not yet been described for *Dlx3* in mice. *Dlx3*-deficient mice die between E9.5 and E10, within a similar time-frame as *Ovol2* mutants; however, the initial study only focused on the placental phenotype of these mice (Morasso et al., 1999). In light of our findings, it should be worthwhile to further explore the *Dlx3* mutant mice to address a likely conserved involvement of *Dlx3* in mammalian neural induction and patterning. The hypothesis that *Ovol2* and *Dlx3* function in a common pathway to position the neuroectoderm/surface ectoderm border and that *Dlx3* is genetically downstream of *Ovol2* should be systematically tested. Furthermore, given that its *ovo* relatives in flies, mice, and human are regulated by BMP and Wnt signaling pathways, *Ovol2* itself might be subject to

regulation by the anti-neural BMP and Wnt signaling in the ectoderm, a notion worth addressing in the future.

Ovol2 and neural crest migration/survival

Neural crest cells emerge from the neuroectoderm/surface ectoderm border, where complex interactions between signaling pathways are thought to be key to neural crest induction and emigration (Gammill and Bronner-Fraser, 2003). It is conceivable that a mispositioned border might result in aberrant tissue and molecular interactions, which could in turn lead to defective neural crest development. Our studies demonstrate that, despite the lateral shift of neuroectoderm/surface ectoderm border in *Ovol2* mutants, neural crest formation is largely unaffected. This result may not be too surprising considering the largely normal levels of expression of *Msx1/2*, presumptive targets of BMP signals from the surface ectoderm, and *Wnt6*, recently proposed to be a major neural crest-inducing signal from the surface ectoderm (Trainor, 2005), in the *Ovol2* embryos. Instead, the emigration of nascent neural crest cells from the neural plate and the survival of migrating neural crest cells were impaired, demonstrating a role for *Ovol2* in these later processes.

How *Ovol2* might regulate neural crest cell migration and survival is another interesting question. Besides its role in promoting neural crest precursor proliferation, Wnt signaling is also implicated in neural crest migration as treatment of cultured neural crest cells with reagents that mimic an activated Wnt signal results in inhibition of migration (de Melker et al., 2004). Therefore, the ventrally expanded *Wnt1* expression of the mutant neuroepithelium may create a stronger source of Wnt signal that inhibits migration of the neural crest cells. Genetic perturbation experiments suggest that neural crest migration and survival is more than just an intrinsic property but rather is controlled non-cell-autonomously by signals from multiple tissues including the surface ectoderm (Trainor, 2005). Since an abundant site of *Ovol2* expression at ~E8.5 is the surface ectoderm, it is likely that *Ovol2* regulates signals originating from the surface ectoderm, which in turn regulate neural crest migration. As the actual signals that regulate cranial neural crest migration in mice (independently of a function in neural crest induction) have not been unequivocally identified (Trainor, 2005), it is difficult to postulate at this time the specific nature of these signals. Furthermore, we cannot rule out the possibility that *Ovol2* is expressed in neural crest cells at a level below our methods of detection and is required autonomously in these cells for their migration and maintenance.

The first two cranial neural crest streams are destined to migrate to the first and second branchial arches, respectively (Kulesa et al., 2004). The branchial arches in the *Ovol2* mutants were consistently less developed than those in the wild type. Although some neural crest cells were able to migrate to and populate the branchial arches in the mutant, the *Sox10*-positive neural crest domain was smaller (Fig. 8 and data not shown), suggesting that branchial arch underdevelopment is at least in part due to neural crest defects. Alternatively, since *Ovol2* is expressed in the surface ectoderm of branchial arches, it is possible that mutant branchial arches fail to emit the necessary signals (e.g., FGFs; Trumpp et al., 1999) to attract or maintain migrating neural crest cells, thus leading to their apoptotic death along the migrating paths and within the branchial arches. Regardless of the underlying mechanism, our findings uncover an important role for *Ovol2* in neural crest cell migration and maintenance, an involvement that is apparently independent of the initial induction event. Unfortunately, the death of *Ovol2* mutant embryos shortly afterwards prevents us from analyzing the neural crest derivatives at later developmental time points. Again, conditional ablation of *Ovol2* will help circumvent this problem.

Ovol2 and cranial neural tube closure

At a morphological level, the cranial neurulation defect in *Ovol2* mutant embryos mimics those observed in mice deficient in *Ptch1* (Goodrich et al., 1997) or Atrophin 2 (Zoltewicz et al., 2004), both associated with abnormal *Shh* expression and/or Shh signaling. While uncontrolled Shh signaling due to the loss of a negative regulator underlies the morphological defect in *Ptch1* mutants, Atrophin 2-deficient embryos display a complete loss of *Shh* expression in the anterior midline. The defect in *Ovol2* mutants, however, is milder and is characterized by an abnormal distribution of *Shh* gene products and signaling activity in the cranial region, creating local domains with either slightly diminished or enhanced Shh signaling activity. The apparent discrepancy between the severe morphological anomaly and mild Shh signaling defect implies the existence of additional factors contributing to a failure of cranial neural closure in the absence of *Ovol2*. The lateral shift of the neuroectoderm/surface ectoderm border in *Ovol2* mutant likely represents one such contributing factor. Morphological defects of cranial neural folds and a disrupted neuroectoderm/surface ectoderm border similar to what we observed in the *Ovol2* mutants have been previously associated with a high incidence of neural tube closure defects in mice (Gunn et al., 1993), providing correlative support for this hypothesis. Another probable cause is the reduced proliferation in *Ovol2* mutant neuroectoderm at E8.5, which might lead to an improper shape of the developing neural plate, thereby creating a physical barrier for its dorsal closure at the anterior end. Finally, the untimely migration of neural crest cells away from the neural plate border and the reduced amount of head mesenchyme likely also contribute to the open brain defects. Collectively, our results demonstrate that *Ovol2* is involved in multiple cellular, molecular, and morphological events required for brain morphogenesis and implicate mice containing *Ovol2* mutations as useful tools to study this important biological process and to model after human diseases with similar brain defects.

Acknowledgments

We would like to thank the UCI Transgenic Mouse Facility and the UCI Optical Biology Core for technical assistance; Bill Skarnes for the generous gift of E14 ES cells; Grant MacGregor for getting us started with embryological techniques; Grant MacGregor and Patrick Tam for helpful suggestions and critical reading of the manuscript; and Marianne Bronner-Fraser, Siew-Lan Ang, Ian Gallicano, Maike Sander, Andy McMahon, Maria Morasso, Alex Joyner, Phil Soriano, Jonathan Epstein, and David Wilkinson for in situ hybridization probes; and reviewers of the manuscript for helpful insights. D.R.M. was supported by an NIH institutional training grant on Structure and Function of Macromolecules. This work was supported by the NIH Research Grant R01 AR47320 and Independent Scientist Award K02 AR51482 awarded to X.D.

References

Altmann CR, Brivanlou AH. Neural patterning in the vertebrate embryo. Int. Rev. Cytol 2001;203:447–482. [PubMed: 11131523]

Anderson RM, Lawrence AR, Stottmann RW, Bachiller D, Klingen-smith J. Chordin and noggin promote organizing centers of forebrain development in the mouse. Development 2002;129:4975–4987. [PubMed: 12397106]

Ang SL, Jin O, Rhinn M, Daigle N, Stevenson L, Rossant J. A targeted mouse Otx2 mutation leads to severe defects in gastrulation and formation of axial mesoderm and to deletion of rostral brain. Development 1996;122:243–252. [PubMed: 8565836]

Bally-Cuif L, Hammerschmidt M. Induction and patterning of neuronal development, and its connection to cell cycle control. Curr. Opin. Neurobiol 2003;13:16–25. [PubMed: 12593978]

Basler K, Edlund T, Jessell TM, Yamada T. Control of cell pattern in the neural tube: regulation of cell differentiation by dorsalin-1, a novel TGF beta family member. Cell 1993;73:687–702. [PubMed: 7916656]

Beanan MJ, Feledy JA, Sargent TD. Regulation of early expression of Dlx3, a *Xenopus* anti-neural factor, by beta-catenin signaling. Mech. Dev 2000;91:227–235. [PubMed: 10704847]

Brennan J, Lu CC, Norris DP, Rodriguez TA, Beddington RS, Robertson EJ. Nodal signalling in the epiblast patterns the early mouse embryo. Nature 2001;411:965–969. [PubMed: 11418863]

Briscoe J, Ericson J. Specification of neuronal fates in the ventral neural tube. Curr. Opin Neurobiol 2001;11:43–49. [PubMed: 11179871]

Camus A, Davidson BP, Billiards S, Khoo P, Rivera-Perez JA, Wakamiya M, Behringer RR, Tam PP. The morphogenetic role of midline mesendoderm and ectoderm in the development of the forebrain and the midbrain of the mouse embryo. Development 2000;127:1799–1813. [PubMed: 10751169]

Catron KM, Wang H, Hu G, Shen MM, Abate-Shen C. Comparison of MSX-1 and MSX-2 suggests a molecular basis for functional redundancy. Mech. Dev 1996;55:185–199. [PubMed: 8861098]

Chamberlin HM, Brown KB, Sternberg PW, Thomas JH. Characterization of seven genes affecting *Caenorhabditis elegans* hindgut development. Genetics 1999;153:731–742. [PubMed: 10511553]

Cheng Y, Cheung M, Abu-Elmagd MM, Orme A, Scotting PJ. Chick sox10, a transcription factor expressed in both early neural crest cells and central nervous system. Brain Res. Dev. Brain Res 2000;121:233–241.

Copp AJ, Greene ND, Murdoch JN. The genetic basis of mammalian neurulation. Nat. Rev., Genet 2003;4:784–793. [PubMed: 13679871]

Dai X, Schonbaum C, Degenstein L, Bai W, Mahowald A, Fuchs E. The ovo gene required for cuticle formation and oogenesis in flies is involved in hair formation and spermatogenesis in mice. Genes Dev 1998;12:3452–3463. [PubMed: 9808631]

Dale JK, Vesque C, Lints TJ, Sampath TK, Furley A, Dodd J, Placzek M. Cooperation of BMP7 and SHH in the induction of forebrain ventral midline cells by prechordal mesoderm. Cell 1997;90:257–269. [PubMed: 9244300]

de Melker AA, Desban N, Duband JL. Cellular localization and signaling activity of beta-catenin in migrating neural crest cells. Dev. Dyn 2004;230:708–726. [PubMed: 15254905]

Dickinson ME, Krumlauf R, McMahon AP. Evidence for a mitogenic effect of Wnt-1 in the developing mammalian central nervous system. Development 1994;120:1453–1471. [PubMed: 8050356]

Dickinson ME, Selleck MA, McMahon AP, Bronner-Fraser M. Dorsalization of the neural tube by the non-neural ectoderm. Development 1995;121:2099–2106. [PubMed: 7635055]

Echelard Y, Epstein DJ, St-Jacques B, Shen L, Mohler J, McMahon JA, McMahon AP. Sonic hedgehog, a member of a family of putative signaling molecules, is implicated in the regulation of CNS polarity. Cell 1993;75:1417–1430. [PubMed: 7916661]

Feledy JA, Beanan MJ, Sandoval JJ, Goodrich JS, Lim JH, Matsuo-Takasaki M, Sato SM, Sargent TD. Inhibitory patterning of the anterior neural plate in *Xenopus* by homeodomain factors Dlx3 and Msx1. Dev. Biol 1999;212:455–464. [PubMed: 10433834]

Fishman MC, Chien KR. Fashioning the vertebrate heart: earliest embryonic decisions. Development 1997;124:2099–2117. [PubMed: 9187138]

Gammill LS, Bronner-Fraser M. Neural crest specification: migrating into genomics. Nat. Rev., Neurosci 2003;4:795–805. [PubMed: 14523379]

Goodrich LV, Johnson RL, Milenkovic L, McMahon JA, Scott MP. Conservation of the hedgehog/patched signaling pathway from flies to mice: induction of a mouse patched gene by Hedgehog. Genes Dev 1996;10:301–312. [PubMed: 8595881]

Goodrich LV, Milenkovic L, Higgins KM, Scott MP. Altered neural cell fates and medulloblastoma in mouse patched mutants. Science 1997;277:1109–1113. [PubMed: 9262482]

Goulding MD, Chalepakis G, Deutsch U, Erselius JR, Gruss P. Pax-3, a novel murine DNA binding protein expressed during early neurogenesis. EMBO J 1991;10:1135–1147. [PubMed: 2022185]

Goulding MD, Lumsden A, Gruss P. Signals from the notochord and floor plate regulate the region-specific expression of two Pax genes in the developing spinal cord. Development 1993;117:1001–1016. [PubMed: 8100762]

Graham A, Francis-West P, Brickell P, Lumsden A. The signalling molecule BMP4 mediates apoptosis in the rhombencephalic neural crest. Nature 1994;372:684–686. [PubMed: 7990961]

Gunn TM, Juriloff DM, Vogl W, Harris MJ, Miller JE. Histological study of the cranial neural folds of mice genetically liable to exencephaly. Teratology 1993;48:459–471. [PubMed: 8303615]

Gurley LR, D'Anna JA, Barham SS, Deaven LL, Tobey RA. Histone phosphorylation and chromatin structure during mitosis in Chinese hamster cells. Eur. J. Biochem 1978;84:1–15. [PubMed: 206429]

Hemmati-Brivanlou A, Melton D. Vertebrate neural induction. Annu. Rev. Neurosci 1997;20:43–60. [PubMed: 9056707]

Ikeya M, Lee SM, Johnson JE, McMahon AP, Takada S. Wnt signalling required for expansion of neural crest and CNS progenitors. Nature 1997;389:966–970. [PubMed: 9353119]

Jacobson AG. Influences of ectoderm and endoderm on heart differentiation in the newt. Dev. Biol 1960;2:138–154. [PubMed: 14406400]

Jessell TM. Neuronal specification in the spinal cord: inductive signals and transcriptional codes. Nat. Rev., Genet 2000;1:20–29. [PubMed: 11262869]

Joyner, AL. Establishment of anterior-posterior and dorsal-ventral pattern in the early central nervous system. In: Rossant, J.; Tam, PPL., editors. Mouse Development. San Diego: Academic Press; 2002. p. 107-126.

Kanzler B, Foreman RK, Labosky PA, Mallo M. BMP signaling is essential for development of skeletogenic and neurogenic cranial neural crest. Development 2000;127:1095–1104. [PubMed: 10662648]

Kowanetz M, Valcourt U, Bergstrom R, Heldin CH, Moustakas A. Id2 and Id3 define the potency of cell proliferation and differentiation responses to transforming growth factor beta and bone morphogenetic protein. Mol. Cell. Biol 2004;24:4241–4254. [PubMed: 15121845]

Kulesa P, Ellies DL, Trainor PA. Comparative analysis of neural crest cell death, migration, and function during vertebrate embryogenesis. Dev. Dyn 2004;229:14–29. [PubMed: 14699574]

Kuo JS, Patel M, Gamse J, Merzdorf C, Liu X, Apekin V, Sive H. Opl: a zinc finger protein that regulates neural determination and patterning in *Xenopus*. Development 1998;125:2867–2882. [PubMed: 9655809]

Lee KJ, Jessell TM. The specification of dorsal cell fates in the vertebrate central nervous system. Annu. Rev. Neurosci 1999;22:261–294. [PubMed: 10202540]

Li B, Dai Q, Li L, Nair M, Mackay D, Dai X. Ovol2, a mammalian homolog of *Drosophila* ovo: gene structure, chromosomal mapping, and aberrant expression in blind-sterile mice. Genomics 2002a; 80:319. [PubMed: 12213202]

Li B, Mackay DR, Dai Q, Li TWH, Nair M, Fallahi M, Schonbaum C, Fantes J, Mahowald A, Waterman ML, Fuchs E, Dai X. The LEF1/b-catenin complex activates movo1, a mouse homolog of *Drosophila* ovo gene required for epidermal appendage differentiation. Proc. Natl. Acad. Sci. U. S. A 2002b;99:6064–6069. [PubMed: 11983900]

Li B, Nair M, Mackay DR, Bilanchone V, Hu M, Fallahi M, Song H, Dai Q, Cohen PE, Dai X. Ovol1 regulates meiotic pachytene progression during spermatogenesis by repressing Id2 expression. Development 2005;132:1463–1473. [PubMed: 15716349]

Liem KF Jr, Tremml G, Roeling H, Jessel TM. Dorsal differentiation of neural plate cells induced by BMP-mediated signals from epidermal ectoderm. Cell 1995;82:969–979. [PubMed: 7553857]

Luo T, Matsuo-Takasaki M, Sargent TD. Distinct roles for Distal-less genes Dlx3 and Dlx5 in regulating ectodermal development in *Xenopus*. Mol. Reprod. Dev 2001;60:331–337. [PubMed: 11599044]

Mahmood R, Bresnick J, Hornbruch A, Mahony C, Morton N, Colquhoun K, Martin P, Lumsden A, Dickson C, Mason I. A role for FGF-8 in the initiation and maintenance of vertebrate limb bud outgrowth. Curr. Biol 1995;5:797–806. [PubMed: 7583127]

Marchant L, Linker C, Ruiz P, Guerrero N, Mayor R. The inductive properties of mesoderm suggest that the neural crest cells are specified by a BMP gradient. Dev. Biol 1998;198:319–329. [PubMed: 9659936]

Mevel-Ninio M, Terracol R, Salles C, Vincent A, Payre F. ovo, a *Drosophila* gene required for ovarian development, is specifically expressed in the germline and shares most of its coding sequences with shavenbaby, a gene involved in embryo patterning. Mech. Dev 1995;49:83–95. [PubMed: 7748792]

Mizuseki K, Kishi M, Matsui M, Nakanishi S, Sasai Y. *Xenopus* Zic-related-1 and Sox-2, two factors induced by chordin, have distinct activities in the initiation of neural induction. Development 1998;125:579–587. [PubMed: 9435279]

Morasso MI, Markova NG, Sargent TD. Regulation of epidermal differentiation by a Distal-less homeodomain gene. J. Cell Biol 1996;135:1879–1887. [PubMed: 8991098]

Morasso MI, Grinberg A, Robinson G, Sargent TD, Mahon KA. Placental failure in mice lacking the homeobox gene Dlx3. Proc. Natl. Acad. Sci. U. S. A 1999;96:162–167. [PubMed: 9874789]

Nagy, A.; Gertsenstein, MG.; Vintersten, K.; Behringer, R. Manipulating the Mouse Embryo. Cold Spring Harbor, NY: Cold Spring Harbor Press; 2003.

Nakata K, Nagai T, Aruga J, Mikoshiba K. *Xenopus* Zic3, a primary regulator both in neural and neural crest development. Proc. Natl. Acad. Sci. U. S. A 1997;94:11980–11985. [PubMed: 9342348]

Nguyen VH, Schmid B, Trout J, Connors SA, Ekker M, Mullins MC. Ventral and lateral regions of the zebrafish gastrula, including the neural crest progenitors, are established by a bmp2b/swirl pathway of genes. Dev. Biol 1998;199:93–110. [PubMed: 9676195]

Oliver B, Singer J, Laget V, Pennetta G, Pauli D. Function of *Drosophila* ovo+ in germ-line sex determination depends on X-chromosome number. Development 1994;120:3185–3195. [PubMed: 7720561]

Parr BA, Shea MJ, Vassileva G, McMahon AP. Mouse Wnt genes exhibit discrete domains of expression in the early embryonic CNS and limb buds. Development 1993;119:247–261. [PubMed: 8275860]

Payre F, Vincent A, Carreno S. ovo/svb integrates Wingless and DER pathways to control epidermis differentiation. Nature 1999;400:271–275. [PubMed: 10421370]

Pusch C, Hustert E, Pfeifer D, Sudbeck P, Kist R, Roe B, Wang Z, Balling R, Blin N, Scherer G. The SOX10/Sox10 gene from human and mouse: sequence, expression, and transactivation by the encoded HMG domain transcription factor. Hum. Genet 1998;103:115–123. [PubMed: 9760192]

Quint E, Zerucha T, Ekker M. Differential expression of orthologous Dlx genes in zebrafish and mice: implications for the evolution of the Dlx homeobox gene family. J. Exp. Zool 2000;288:235–241. [PubMed: 11069141]

Robinson GW, Mahon KA. Differential and overlapping expression domains of Dlx-2 and Dlx-3 suggest distinct roles for Distal-less homeobox genes in craniofacial development. Mech. Dev 1994;48:199–215. [PubMed: 7893603]

Rubenstein JL, Beachy PA. Patterning of the embryonic forebrain. Curr. Opin. Neurobiol 1998;8:18–26. [PubMed: 9568388]

Saint-Jeannet JP, He X, Varmus HE, Dawid IB. Regulation of dorsal fate in the neuraxis by Wnt-1 and Wnt-3a. Proc. Natl. Acad. Sci. U. S. A 1997;94:13713–13718. [PubMed: 9391091]

Sambrook, R.; Russell, DW. Molecular Cloning. Cold Spring Harbor NY: Cold Spring Harbor Press; 2001.

Shimamura K, Rubenstein JL. Inductive interactions direct early regionalization of the mouse forebrain. Development 1997;124:2709–2718. [PubMed: 9226442]

Smith JL, Schoenwolf GC. Neurulation: coming to closure. Trends Neurosci 1997;20:510–517. [PubMed: 9364665]

Stoller JZ, Epstein JA. Cardiac neural crest. Semin. Cell Dev. Biol 2005;16:704–715. [PubMed: 16054405]

Suzuki A, Ueno N, Hemmati-Brivanlou A. *Xenopus* msx1 mediates epidermal induction and neural inhibition by BMP4. Development 1997;124:3037–3044. [PubMed: 9272945]

Trainor PA. Specification of neural crest cell formation and migration in mouse embryos. Semin. Cell Dev. Biol 2005;16:683–693. [PubMed: 16043371]

Trainor PA, Sobieszczuk D, Wilkinson D, Krumlauf R. Signalling between the hindbrain and paraxial tissues dictates neural crest migration pathways. Development 2002;129:433–442. [PubMed: 11807035]

Trumpp A, Depew MJ, Rubenstein JL, Bishop JM, Martin GR. Cre-mediated gene inactivation demonstrates that FGF8 is required for cell survival and patterning of the first branchial arch. Genes Dev 1999;13:3136–3148. [PubMed: 10601039]

Wilkinson DG, Bhatt S, Chavrier P, Bravo R, Charnay P. Segment-specific expression of a zinc-finger gene in the developing nervous system of the mouse. Nature 1989;337:461–464. [PubMed: 2915691]

Wilson SW, Houart C. Early steps in the development of the forebrain. Dev. Cell 2004;6:167–181. [PubMed: 14960272]

Wilson PA, Lagna G, Suzuki A, Hemmati-Brivanlou A. Concentration-dependent patterning of the *Xenopus* ectoderm by BMP4 and its signal transducer Smad1. Development 1997;124:3177–3184. [PubMed: 9272958]

Wilson SI, Rydstrom A, Trimborn T, Willert K, Nusse R, Jessell TM, Edlund T. The status of Wnt signalling regulates neural and epidermal fates in the chick embryo. Nature 2001;411:325–330. [PubMed: 11357137]

Wittler L, Kessel M. The acquisition of neural fate in the chick. Mech. Dev 2004;121:1031–1042. [PubMed: 15296969]

Woda JM, Pastagia J, Mercola M, Artinger KB. Dlx proteins position the neural plate border and determine adjacent cell fates. Development 2003;130:331–342. [PubMed: 12466200]

Zoltewicz JS, Stewart NJ, Leung R, Peterson AS. Atrophin 2 recruits histone deacetylase and is required for the function of multiple signaling centers during mouse embryogenesis. Development 2004;131:3–14. [PubMed: 14645126]

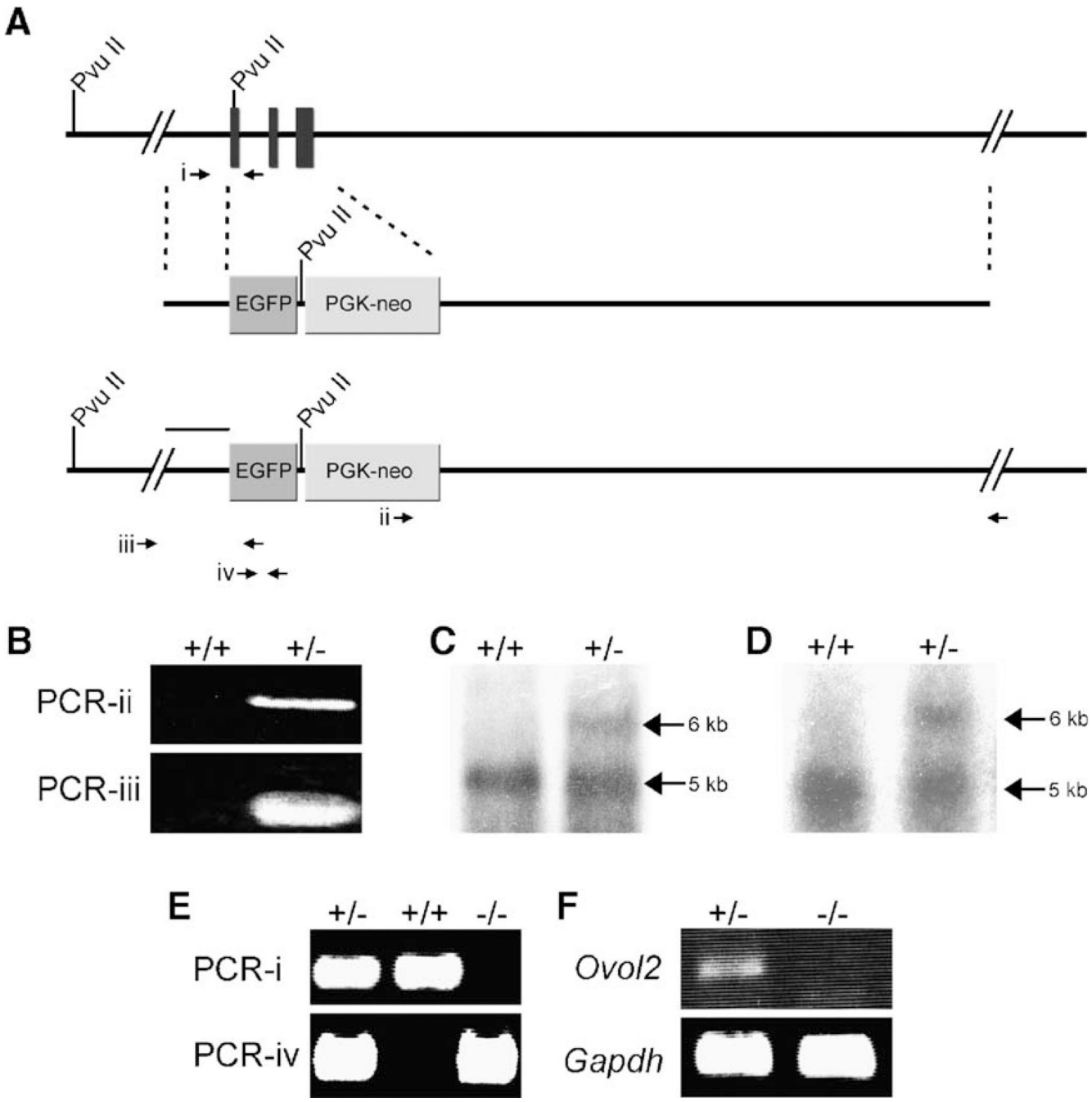

Fig. 1.

Targeted deletion of *Ovol2*. (A) Targeting vector design and the resulting mutant allele. (B) PCR genotype results using the primer sets indicated by arrows in (A) demonstrated the proper targeting at the *Ovol2* locus in ES cells. (C–D) Southern blot analysis of DNA isolated from either targeted ES cells (C) or tail clippings from heterozygous mice (D) using the probe indicated by the bar above the recombined allele. (E) PCR analysis of yolk sac DNA isolated from embryos at E8.5. (F) RT-PCR analysis on RNA isolated from embryos at E9.5 demonstrated that *Ovol2* expression was disrupted as designed.

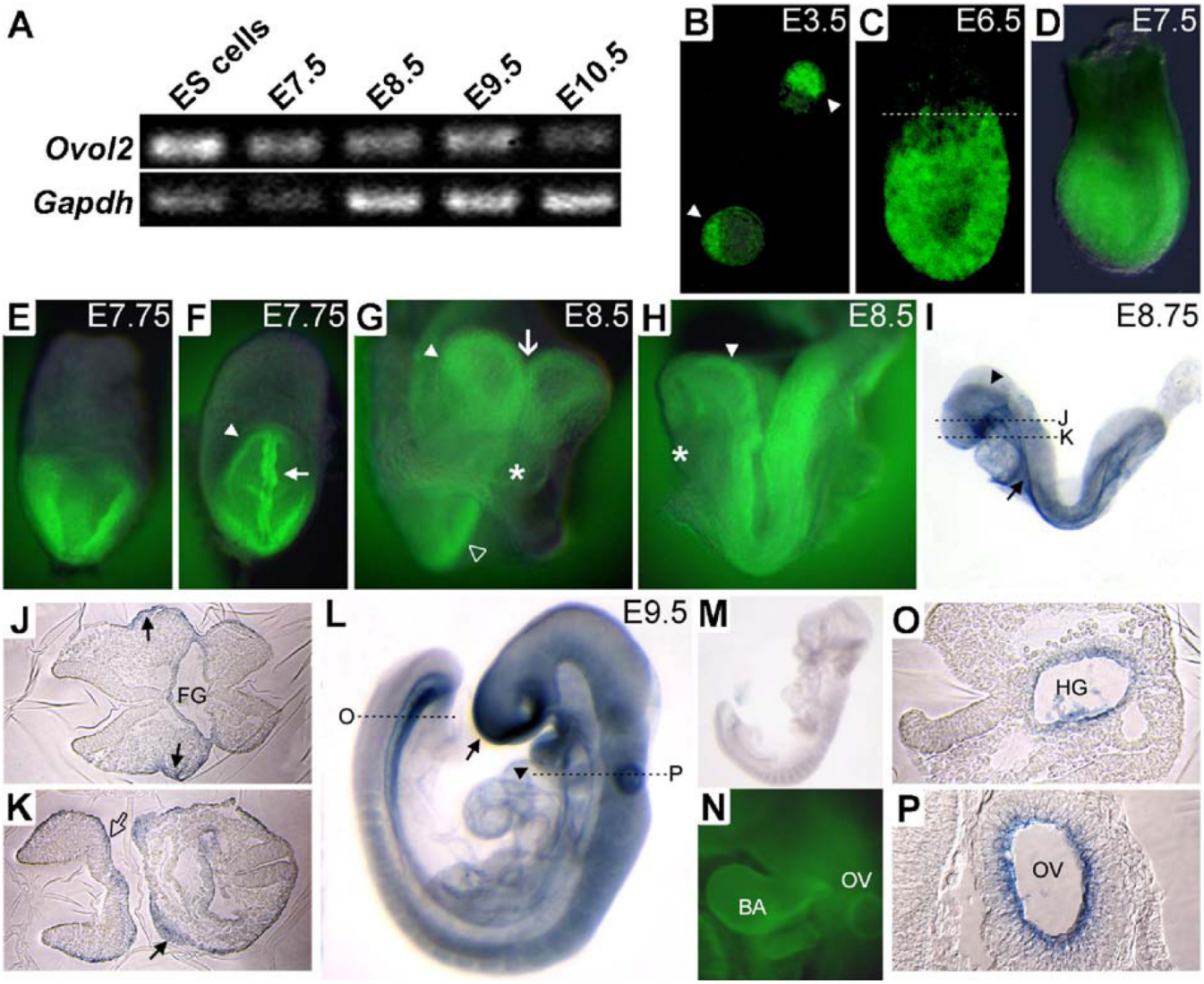

Fig. 2.

Expression of *Ovol2* during early–mid embryogenesis. (A) RT-PCR analysis of *Ovol2* expression at the stages indicated. (B) Epifluorescence analysis of blastocyst stage heterozygous embryos. Arrowheads indicate inner cell mass. (C) Confocal microscopy analysis of an E6.5 embryo. (D–H) Epifluorescence images of EGFP expression merged with corresponding brightfield images at E7.5 (D), E7.75 (E–F), and E8.5 (G–H). F and G represent an anterior view of the embryos in E and H, respectively. (I) Whole mount in situ hybridization at E8.75 using an *Ovol2* antisense probe. Arrow indicates the gut tube, and arrowhead indicates surface ectoderm next to the neural plate. No signal was detected using the same probe on stage-matched *Ovol2*-deficient embryos (not shown). (J–K) Sections through the planes indicated in (I) confirmed *Ovol2* expression in the ectodermal component of the branchial arches (arrows) and in the surface ectoderm of the forebrain region (open arrow). (L) At E9.5, *Ovol2* expression persisted in the embryonic gut (see section in O) and branchial arches (BA) (arrowhead), and enhanced expression was seen in the forebrain region (arrow) and otic vesicles (OV) (see section in P). (M) *Ovol2* in situ hybridization using E9.5 *Ovol2*-deficient embryos. (N) EGFP expression at E9.5 in the BA and OV. (O–P) sections through the planes indicated in L. FG, foregut; HG, hindgut.

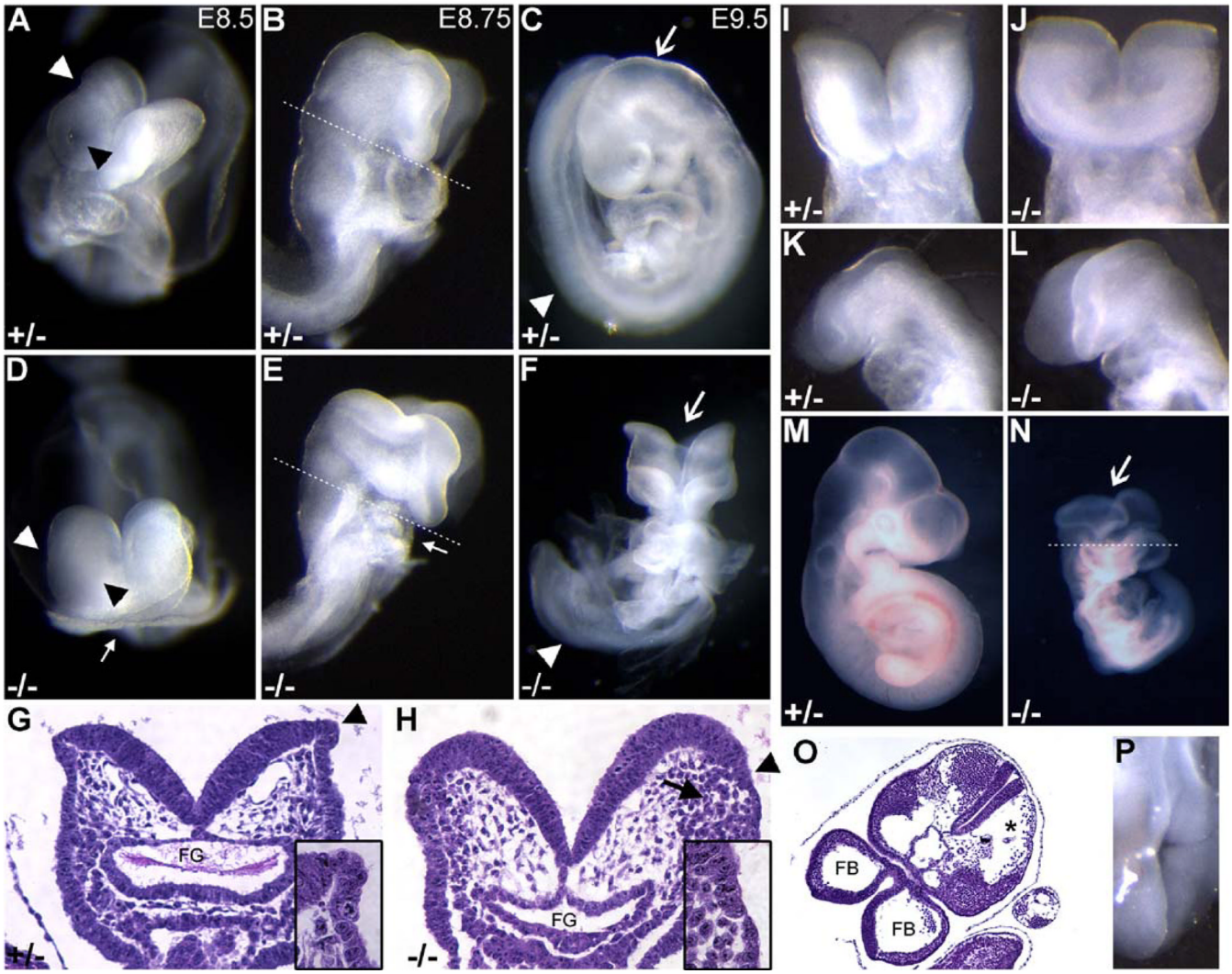

Fig. 3.

Morphological defects of the *Ovol2* mutant embryos. Morphological comparison of control (A–C) and mutant (D–F) B6 × 129 embryos at the indicated stages. (A, D) Morphology at E8.5. Note the absence of a heart in this mutant embryo (arrow). (B, E) Slightly later in development, the defects in the presumptive brain and heart became more apparent. (C, F) At E9.5, the cranial neural tube region of the mutant embryos was still open (arrow). Note the twisted appearance of the trunk in (F) (arrowhead). (G–H) Histological sections through the hindbrain region of E8.75 embryos as indicated in (B) and (E). The arrowheads demarcate the neuroectoderm/surface ectoderm junction. The arrow in (H) indicates cells with neural crest cell morphology in closer proximity to the neuroectoderm/surface ectoderm border in the mutant. Inset panels in (G) and (H) represent higher magnification images of the neuroectoderm/surface ectoderm transition. FG, foregut. (I–P) Morphological analysis of E8.5 (I–L) and E9.5 (M–P) embryos in the CD1-enriched genetic background. Ventral (I–J) and lateral (K–L) views of control and mutant embryos at E8.5 revealed enlarged, round neural folds in the mutant. Note the open cranial neural tube (arrow) in the mutant at E9.5 (N). (O) Section through the cranial region of a mutant embryo (plane of cleavage is indicated in N). FB, forebrain. (P) Dorsal view of the trunk region of an “escaper” that displayed spina bifida.

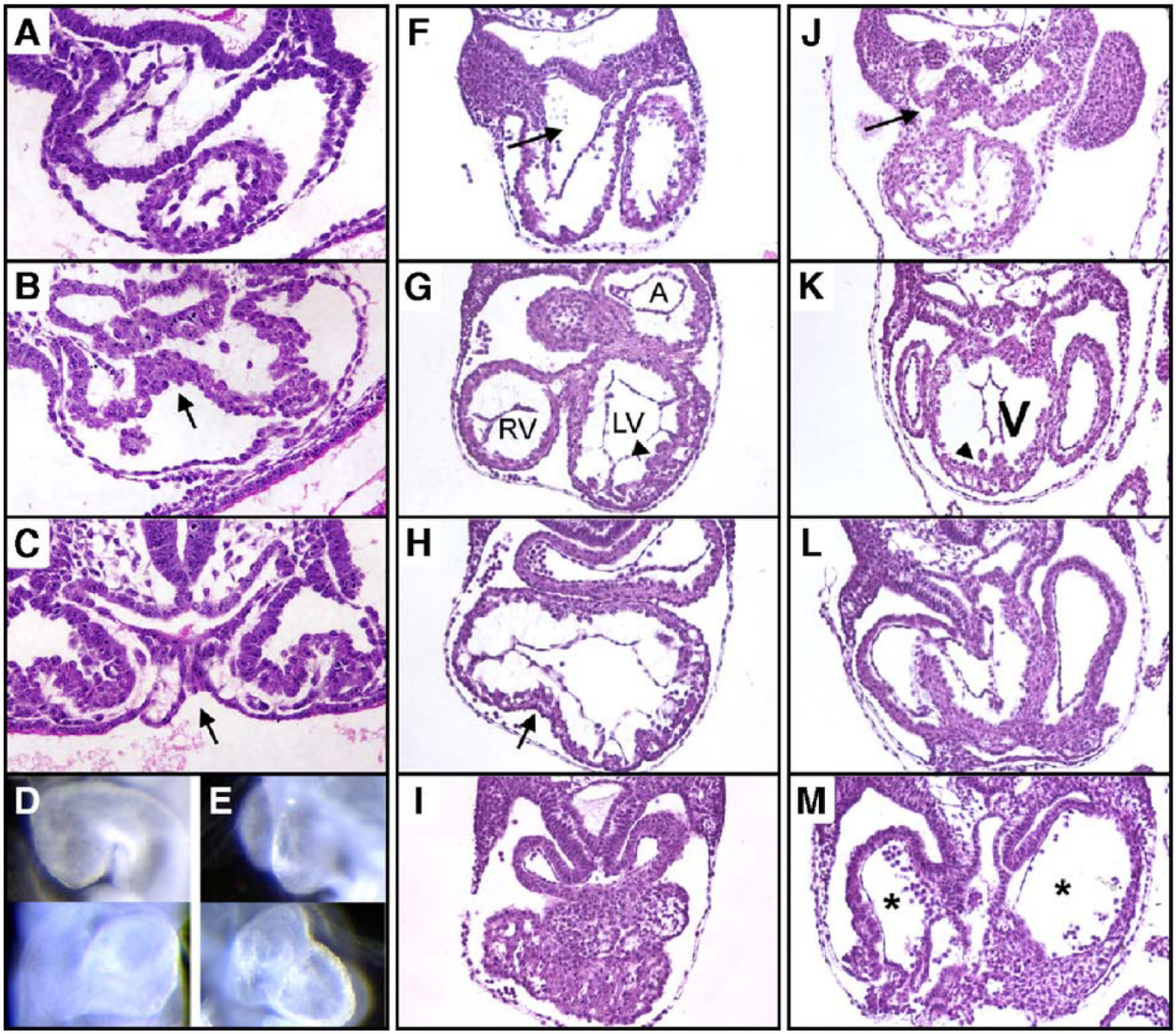

Fig. 4.

Heart defects in *Ovol2* mutants. (A–C) Transverse sections through comparable regions of wild-type (A) and *Ovol2* mutant embryos (B–C) at E8.5 illustrating a range of severity of disrupted heart development in the mutants. Arrows indicate regions where the two primordial heart fields have failed to fuse. (D–E) Lateral (top) and frontal (bottom) views of wild-type (D) and mutant (E) hearts at E9.5. (F–M) A series of sections through wild-type (F–I) and mutant (J–M) hearts at E9.5. The wild-type sections span a greater distance than those of the mutant. Arrowheads in (G) and (K) indicate trabeculated myocardium. Arrow in panel H indicates that septation between the future right and left ventricles that is not observed in the mutant. A, atrium; RV, right ventricle; LV, left ventricle; V, ventricle.

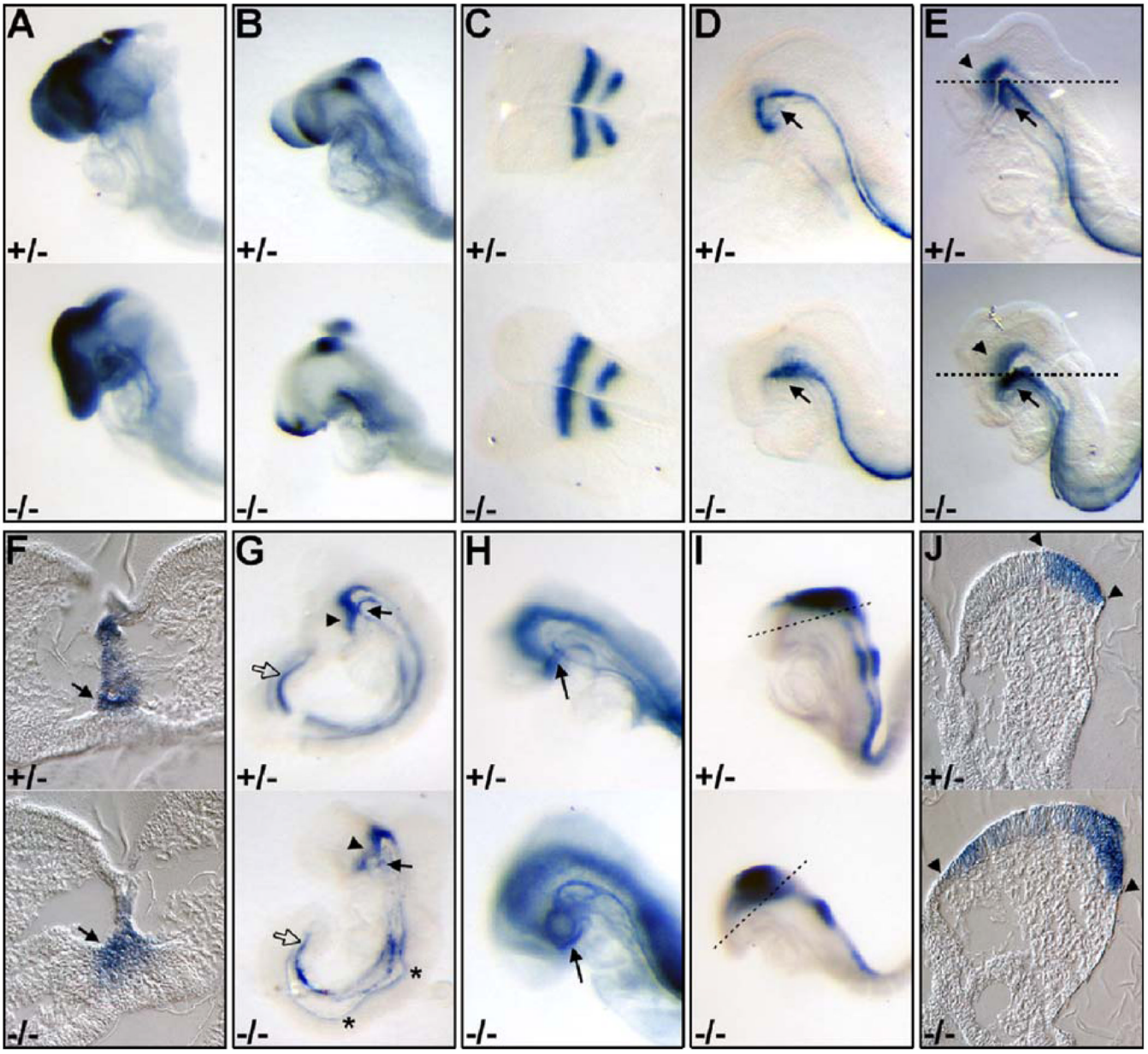

Fig. 5.

Expression analysis of signaling centers involved in brain patterning. (A) *Otx2*, (B) *Fgf8*, and (C) *Krox20* expression confirmed largely normal A–P brain patterning in the E8.5 mutants. (D–E) *Shh* expression at E8.5 (D) and E8.75 (E). Note weaker expression in the ventral forebrain (arrowhead) of *Ovol2* mutants. (F) Sections through the cranial region of the embryos as indicated in panel E. Arrows indicate *Shh* expression in prechordal plate. (G) *Shh* expression at E9.5. Note the reduced expression in mutant prechordal plate (arrow). (H) *Ptch1* expression at E8.75. (I) *Wnt1* expression at E8.5. (J) Sections through the cranial region of the embryos indicated in I, with arrowheads marking the domain of expression.

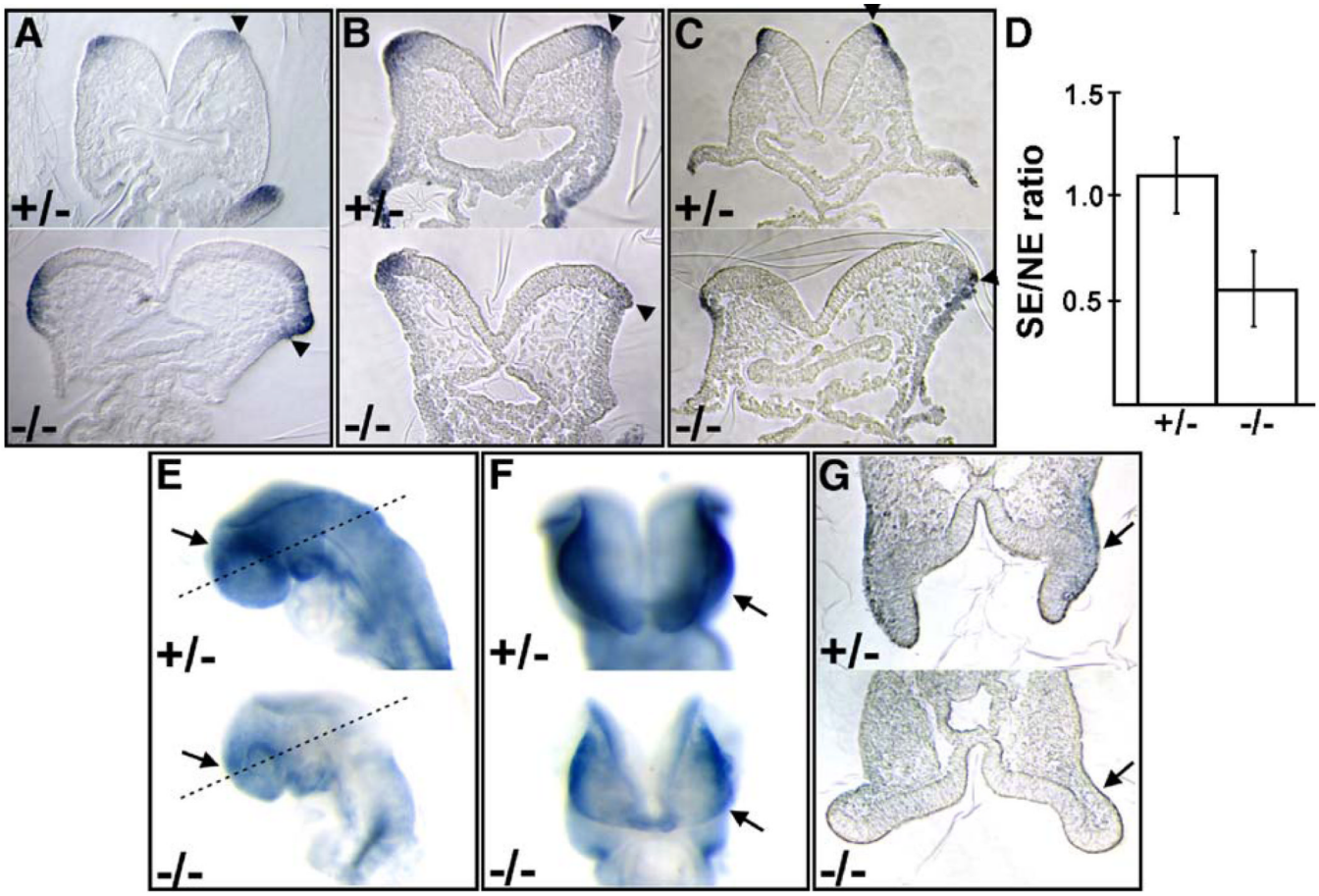

Fig. 6.

The lateral shift of the neuroectoderm/surface ectoderm border in *Ovol2* mutant embryos is the result of expanded neuroectoderm and reduced surface ectoderm. (A–C) Transverse sections through embryos hybridized with *Pax3* (A), *Msx2* (B), and *Wnt6* (C) probes. Arrowheads in panels A–C indicate the position of the neuroectoderm/surface ectoderm border. (D) Quantitative analysis of the ratio between surface ectoderm (SE) and neuroectoderm (NE) in control and mutant embryos. Bars represent average ratio determined from 11 control and 11 mutant sections through comparable cranial regions of a total of four embryos of each genotype. (E–F) Whole mount in situ hybridization using a *Dlx3* probe. Lateral (E) and ventral (F) views are shown. Arrows indicate expression in the forebrain region of the control embryos that was weaker in the mutant. (F) Sections through different embryo pairs at planes indicated in panel D. *Dlx3* was expressed in the surface ectoderm of control, but not mutant embryos (arrows).

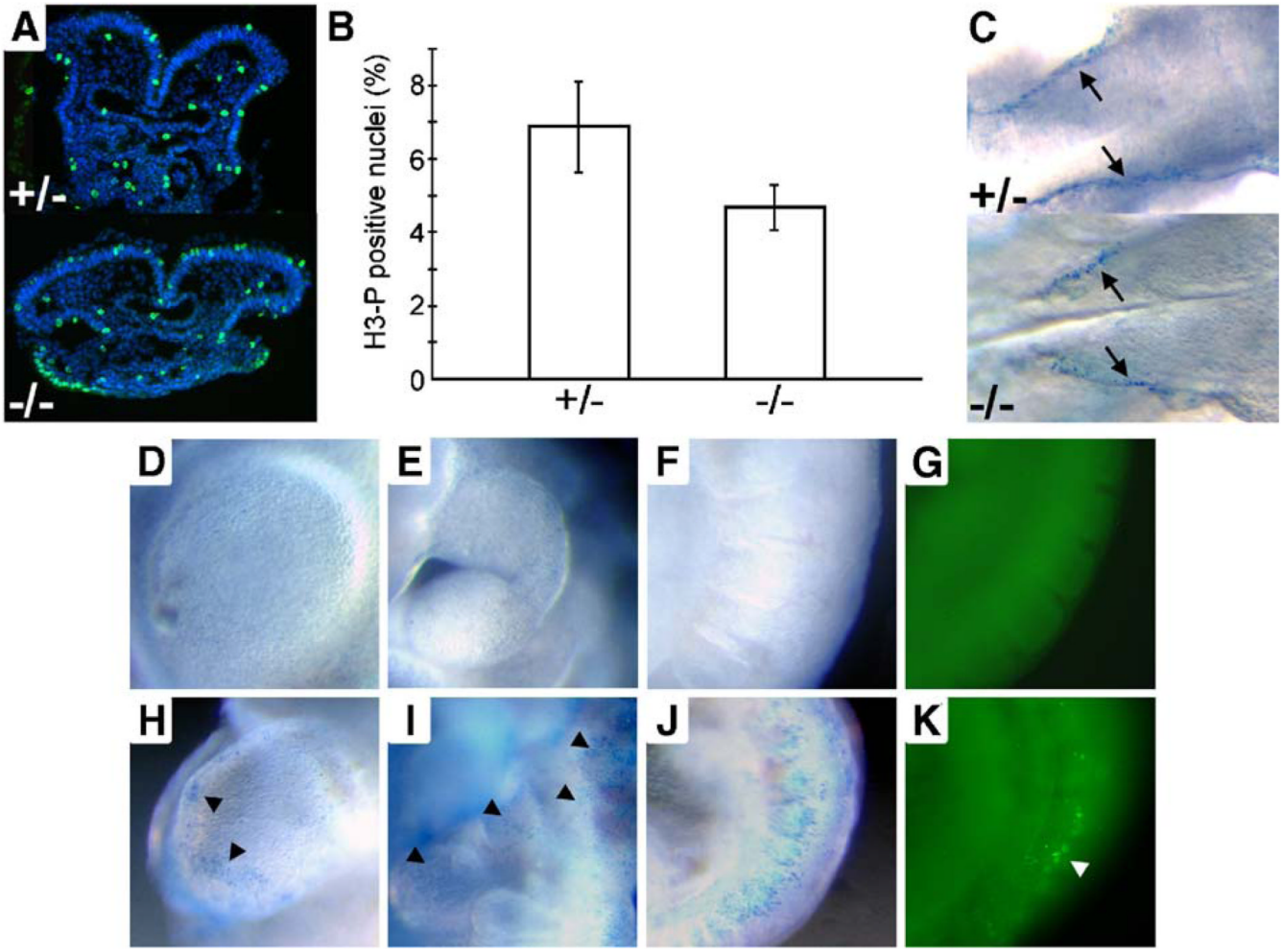

Fig. 7.

Reduced proliferation within the neuroectoderm and increased apoptosis in regions containing migrating neural crest cells. (A) Overlaid images of sections through the cranial region of embryos at E8.5 stained for phosphorylated histone H3 (green) or DAPI (blue). (B) Calculation of the average mitotic index. (C) Nile blue staining of embryos at E8.5. Arrows indicate apoptotic cells along the neuroectoderm/surface ectoderm border. (D–F) Wild-type and (H–J) mutant embryos stained with Nile blue sulfate at E9.5 revealed an increase in apoptosis in the forebrain (D, H), branchial arch (E, I), and trunk (F, J) regions of the mutant embryos. Black arrowheads indicate regions of increased apoptosis. (G, K) TUNEL analysis confirmed the presence of increased apoptosis in the trunk region of the mutant (white arrowhead in panel H).

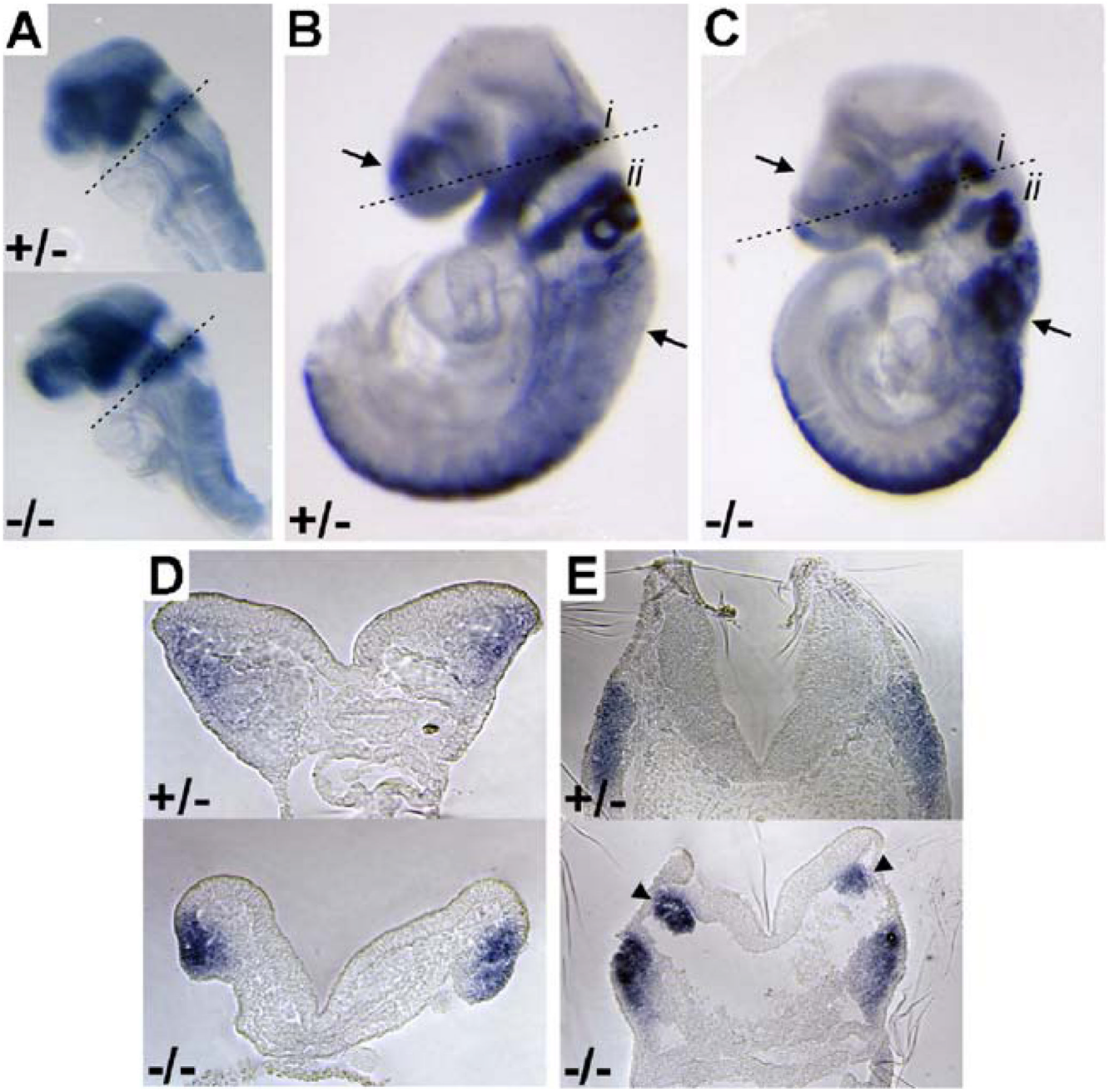

Fig. 8.

Neural crest cells are formed in the mutant but display impaired migration. (A–C) In situ hybridization of embryos at E8.75 (A) and E9.5 (B–C) using a *Sox10* probe. i, neural crest cells migrating into the first branchial arch; ii, neural crest cells migrating into the second branchial arch. (D–E) Sections through the cranial regions of E8.5 (D) and E9.5 (E) embryos hybridized with a *Sox10* probe, with planes of cleavage indicated in panel A–C.

Table 1

Genotyping data of progeny from heterozygote intercrosses

Stage	# of mice	Genotype		
		+/+	+/−	−/−
P14 [a]	161	57	104	0
P14 [b]	53	19	34	0
E11.5–13.5	57	18	39	0
E10.5	15	2	8	5 [c]
E9.5	173	41	91	41
E8.5	542	140	271	131
E7.5	48	14	25	9

[a] C57BL6/J×129Ola genetic background.

[b] CD1-enriched genetic background.

[c] Embryos were in the final stages of resorption.